H_∞ Control Design for a Seeker Scan Loop System

Ho-Pyeong Lee*

(*Received February 20, 1997*)

Two H_∞ Controllers are presented for a seeker scan loop system which has model uncertainty and is subject to external disturbance. The controllers are designed using a new H_∞ control framework formulated by combining the mixed sensitivity and model matching approaches for one- and two-degree-of-freedom control structures. The proposed control methods are able to reflect not only frequency domain specifications but also time domain ones such as transient response characteristics and multivariable interaction between output channels, contrary to the mixed sensitivity problem. It is shown that the two-degree-of-freedom H_∞ controller offers better performance and robustness than one-degree-of-freedom H_∞ controller, but both controllers are very effective for the seeker scan loop system.

Key Words: H_∞ Controllers, Seeker Scan Loop System, One- and Two-Degree-of-Freedom Control Structures, Model Matching

1. Introduction

The target lock-on during the flight after the missile launch has been widely used in order to extend the lock-on range of short range homing missiles. Because a missile seeker has a narrow field-of-view (FOV), the seeker scan loop system searches for a target during flight by making the spinning axis of the seeker follow scanning commands of missile guidance unit for achieving a good acquisition of a target within its FOV. Therefore, the target acquisition probability of a missile is affected by the pointing and scanning accuracies of the seeker. There are two main factors that degrade the accuracy of the seeker scan loop system, *i. e.,* disturbances and modeling uncertainties. Firstly, the firing impulse, dynamic unbalance of the spinning gyro, and a large lateral acceleration during the missile maneuvering act as disturbances on the seeker scan loop system. Secondly, modelling error due to the base-band modelling procedure reduces the stability margin of the scan loop system. In addition to these points, as the seeker scan loop system is composed of high spinning gyro with nonlinear dynamics and the driving electronics modulated in spinning frequency, it is very difficult to obtain an accurate mathematical model. Therefore, to improve the target acquisition probability of a missile in the presence of the disturbances and model uncertainties, it is essential to introduce robust control methodologies (Hwang et al., 1993).

H_∞ optimization theory is developing rapidly in the robust control research (Zames, 1981; Doyle et al. 1989). The mixed sensitivity problem which is widely used in H_∞ optimization hardly capture important objectives such as *multivariable interaction,* and causes the unnecessary *pole-zero cancellation* (Tsai et al., 1992). Also, this method leads to unbalanced input and output performance and robustness properties, and therefore it may be ineffective if, for instance, performances are needed at the output of the plant while robustness is required at the input (Mammar et al., 1992). The idea of the model matching problem is to design a stabilizing controller so that the output of the closed-loop system follows the output of a desired model (Ho. et al., 1992). The desired model is generally chosen considering the

* Senior Researcher, Agency for Defense Development, P. O. Box 35-4 Yuseong, Taejon 305-600, Korea

low multivariable interaction requirement. The closed-loop system resulting from a minimal H_∞ model matching problem, however, may have poor stability robustness.

The main goals of this paper are to propose two H_∞ controllers for a seeker scan loop system in order to improve the scanning performances. The controllers are designed in the framework of the standard H_∞ optimization problem by combining the mixed sensitivity and model matching problems for one- and two-degree-of-freedom control structures. Several performances for a seeker scan loop system are evaluated and, in particular, scanning performances are investigated intensively.

2. Seeker Scan Loop Dynamics

Figure 1 shows the conceptional description for obtaining a mathematical model of the seeker scan loop system.

The seeker scan loop system is composed of a spinning gyro-optics assembly and related signal processors. Because the gyro is spinning with a constant angular rate for the purpose of a stable pointing capability, the carrier frequency of every signal processor is synchronized with the gyro spinning frequency. The modulator converts two control input signals in the pitch-yaw plane which are piecewise constants between two sampling instants into a rectangular wave. Because the frequency components of a rectangular signal consist of the integer multiple of the fundamental frequency, only the fundamental frequency which coincides with the gyro spin frequency passes through band pass filter (BPF). The precession amplifier converts the BPF output voltage into the current which is proportional to the precession torque to the gyro. The voltage which is induced in the solenoidal coils around the gyro rotor magnet is proportional to the component of the velocity of the magnetic pole of the rotor along the centerline of the solenoid. The measured gyro position by the cage coil is the sinusoidal wave form, which represents the magnitude and phase in polar coordinate. The sinusoidal signal is demodulated to two DC magnitudes in pitch-yaw plane. The gyro driving signal generator makes two control inputs at the controller block from angle errors between external pointing or scanning commands and the measured position of the gyro spinning axis in the pitch and yaw directions. These control inputs are modulated in the polar form with the gyro spinning frequency. The mathematical equations of all signal processors have been fully described by Hwang and Lee (1993). In Fig. 1, the dynamic equations of the gyro can be described as follows:

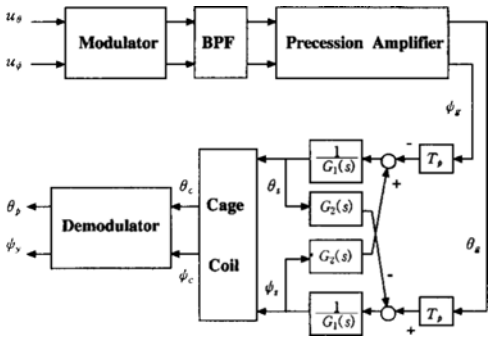

Fig. 1 Open-loop configuration of a seeker scan loop.

$$G_1(s)\,\theta_s(s) = G_2(s)\,\psi_s(s) - T_p\psi_g(s) \quad (1)$$

$$G_1(s)\,\psi_s(s) = -G_2(s)\,\theta_s(s) + T_p\theta_g(s) \quad (2)$$

$$G_1(s) = Is^2 + Ds + K \quad (3)$$

$$G_2(s) = Hs \quad (4)$$

where I, D, K denote the inertia, the damping constant, and the direct-axis spring constant of the gyro; H is the angular momentum of the gyro; T_P is the precession torque constant; $\theta_s(\cdot)$ and $\psi_s(\cdot)$ denote the gyro gimbal angle in the pitch and yaw axes; $\theta_g(\cdot)$ and $\psi_g(\cdot)$ denote the input current proportional to the precession torque in the pitch and yaw axes, respectively. A state-space representation of the seeker scan loop system is given by (Hwang et al., 1993)

$$\dot{x}(t) = Ax(t) + Bu(t) \quad (5)$$

$$y(t) = Cx(t) \quad (6)$$

where the system matrices $A \in R^{10\times 10}$, $B \in R^{15\times 2}$, and $C \in R^{2\times 10}$ are:

$$A=\begin{bmatrix} -50.3 & 0 & 0 & 0 & 0 & 0 & 0 & 0 & 0 & 0 \\ 0 & 0 & 0 & 0 & 0 & 0 & 23.2 & -23.2 & 0 & 0 \\ 183 & 267 & -267 & 0 & 0 & 0 & -902 & 902 & 0 & 0 \\ 0 & 0 & 0 & 0 & 1 & 0 & 0 & 0 & 0 & 0 \\ 0 & 0 & 89673 & -4891 & -140 & 0 & 0 & 0 & 0 & 0 \\ 0 & 0 & 0 & 0 & 0 & -50.3 & 0 & 0 & 0 & 0 \\ 0 & -23.2 & 23.2 & 0 & 0 & 0 & 0 & 0 & 0 & 0 \\ 0 & 902 & -902 & 0 & 0 & 183 & 267 & -267 & 0 & 0 \\ 0 & 0 & 0 & 0 & 0 & 0 & 0 & 0 & 0 & 1 \\ 0 & 0 & 0 & 0 & 0 & 0 & 0 & 89673 & -4891 & -140 \end{bmatrix}$$

$$B^T=\begin{bmatrix} 3.7624 & 0 & 0 & 0 & 0 & 0 & 0 & 0 & 0 & 0 \\ 0 & 0 & 0 & 0 & 0 & 3.7624 & 0 & 0 & 0 & 0 \end{bmatrix}'$$

$$C=\begin{bmatrix} 0 & 0 & 0 & 1 & 0 & 0 & 0 & 0 & 0 & 0 \\ 0 & 0 & 0 & 0 & 0 & 0 & 0 & 1 & 0 & 0 \end{bmatrix}'$$

$x(t)=[\theta_g\ \theta_s\ \theta_c\ \theta_p\ \dot{\theta}_p\ \psi_g\ \psi_s\ \psi_c\ \psi_y\ \dot{\psi}_y]^T$,
$u(t)=[u_\theta\ u_\psi]^T$, $y(t)=[\theta_p\ \psi_y]^T$.

The linear model of the seeker scan loop includes 10 state variables, and two-input and two-output variables, where the states are :

θ_g, ψ_g: currents proportional to the precession torque in the pitch and yaw axes (A)

θ_s, ψ_s: gyro gimbal angles in the pitch and yaw axes (deg)

$\dot{\theta}_s$, $\dot{\psi}_s$: gyro angular rates in the pitch and yaw axes (deg/s)

θ_p, ψ_y: demodulator outputs in the pitch and yaw axes (V)

$\dot{\theta}_p$, $\dot{\psi}_y$: derivative of the demodulator outputs in the pitch and yaw axes (V/s),

and the input and output variables are

u_θ, u_ψ: control inputs in the pitch and yaw axes (V)

θ_p, ψ_y: plants output in the pitch and yaw axes (V).

The seeker scan loop model is both controllable and observable. The seeker scan loop has an integrator in both the pitch and yaw channels, and hence the zero steady state errors are expected to position commands for the closed-loop system. Due to the dynamics of the gyro and cage coil, the interaction between the pitch and yaw channels occurs. The plant zeros are at $\pm 23.2j$ and the poles are at 0, 0, -50.3, -50.3, -68.5, -68.5, -71.4, -71.4, $-267\pm 925j$.

3. H_∞ Optimization Problem with Model Matching

3.1 One-degree-of-freedom H_∞ control problem

Figure 2 shows one-degree-of-freedom H_∞ control problem including model matching.

All weighting functions have deep influence on the performance and stability of the closed-loop system. The desired closed-loop model, T_m is chosen considering design requirements in the time-domain such as overshoot and settling time. The choice of T_m is dictated by specific control design problems and relies on the experience of designer. The rule of thumb is that the dynamics should be simple with low order. In Fig. 2, the controlled output

$$y_G=GS_iKW_r r+GS_iW_d d-GS_iKW_n n \quad (7)$$

$$u=S_iKW_r r-S_iKGW_d d-SKW_n n \quad (8)$$

where $S_i=(I+KG)^{-1}$

The elements of the vector, z, which is to be minimized for better performance of the control system, are given by

$$z_1=W_1(T_mW_r r-y_G)$$

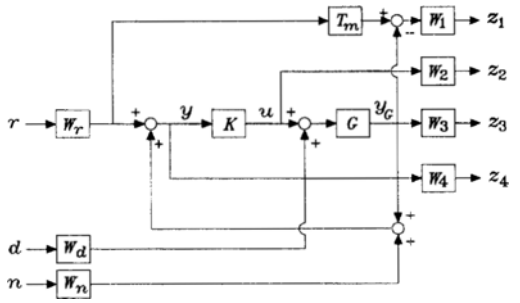

Fig. 2 One-degree-of-freedom H_∞ control problem.

$$= W_1(T_m - GS_iK)W_r r - W_1GS_iW_d d + W_1GS_iKW_n n \quad (9)$$

$$z_2 = W_2 u = W_2S_iKW_r r - W_2S_iKGW_d d - W_2S_iKW_n n \quad (10)$$

$$z_3 = W_3 y_G = W_3GS_iKW_r r + W_3GS_iW_d d - W_3GS_iKW_n n \quad (11)$$

$$z_4 = W_4(W_r r - y_G + W_n n) = W_4(I - GS_iK)W_r r - W_4GS_iW_d d - W_4(I - GS_iK)W_n n \quad (12)$$

Using Eqs. (9)—(12), we obtain the cost transfer function from $w = [r^T\ d^T\ n^T]^T$ to $z = [z_1^T\ z_2^T\ z_3^T\ z_4^T]^T$ as

$$T_{zw} = \begin{bmatrix} W_1(T_m - GS_iK)W_r & -W_1GS_iW_d & W_1GS_iKW_n \\ W_2S_iKW_r & -W_2KGS_iW_d & -W_2S_iKW_n \\ W_3GS_iKW_r & W_3GS_iW_d & -W_3GS_iKW_n \\ W_4(I - GS_iK)W_r & -W_4GS_iW_d & -W_4(I - GS_iK)W_n \end{bmatrix} \quad (13)$$

The remaining work is how to formulate the proposed H_∞ control problem into the framework of the standard H_∞ optimization problem shown in Fig. 3.

In Fig 3, w is a vector of all the signals entering the system which include the reference input, the disturbance and the sensor noise. z is a vector of all the signals to possibly characterize the behavior of the closed-loop system. u is the vector of control signals, and y is the vector of measured outputs.

The standard H_∞ optimization problem is to find a stabilizing controller such that

$$\text{minimize} \| F_l(P, K) \|_\infty \quad (14)$$

whrer $F_l(P, K) = P_{11} + P_{12}(I - KP_{22})^{-1}KP_{21}$, (15)

$$P = \begin{bmatrix} P_{11} & P_{12} \\ P_{21} & P_{22} \end{bmatrix} \quad (16)$$

Note that the transfer functions P_{11}, P_{12}, P_{21} and P_{22} are derived from the plant dynamics, weighting functions for the signals z and w, and the desired closed-loop model.

The design objective is to obtain an internally stabilizing controller K such that

$$\| F_l(P, K) \|_\infty < \gamma \quad (17)$$

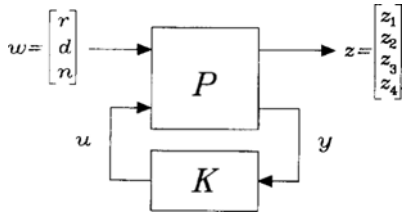

Fig. 3 Linear fractional transformation.

where $\gamma > \gamma_{\min}$ and

$$\gamma_{\min} = \inf_{\text{stabilizing } K} \| F_l(P, K) \|_\infty \quad (18)$$

Since we do not know $\gamma_{\min}$ in advance, the parameter γ is obtained in an iterative manner until a suitable design is achieved.

If we represent Eq. (13) into linear fractional transformation shown in Fig. 3, the elements of P are given by

$$P_{11} = \begin{bmatrix} W_1T_mW_r & -W_1GW_d & 0 \\ 0 & 0 & 0 \\ 0 & W_3GW_d & 0 \\ W_4W_r & -W_4GW_d & -W_4W_n \end{bmatrix},$$

$$P_{12} = \begin{bmatrix} -W_1G \\ W_2 \\ W_3G \\ -W_4G \end{bmatrix},$$

$$P_{21} = [W_r - GW_d\ \ -W_n],\ P_{22} = [-G] \quad (19)$$

Therefore, the proposed H_∞ control problem can be formulated as the standard H_∞ optimization problem. For the stabilizing controllers for Eq. (19), DGKF algorithm (Doyle et al., 1989) provides very simple state-space formulas for all stabilizing controllers by solving two algebraic Riccati equations, once Eq. (19) is represented as a state space realization.

If we define

$$T_m = C_m(sI - A_m)^{-1}B_m + D_m \quad (20)$$

$$G = C_p(sI - A_p)^{-1}B_p + D_p \quad (21)$$

$$W_i = C_{wi}(sI - A_{wi})^{-1}B_{wi} + D_{wi},\ i = 1, 2, 3, 4 \quad (22)$$

$$W_r = C_{wr}(sI - A_{wr})^{-1}B_{wr} + D_{wr} \quad (23)$$

$$W_d = C_{wd}(sI - A_{wd})^{-1}B_{wd} + D_{wd} \quad (24)$$

$$W_n = C_{wn}(sI - A_{wn})^{-1}B_{wn} + D_{wn} \quad (25)$$

then a state space realization of P is given by

$$\dot{x}(t) = Ax(t) + B_1 w(t) + B_2 u(t) \quad (26)$$

$$z(t) = C_1 x(t) + D_{11} w(t) + D_{12} u(t) \quad (27)$$

$$y(t) = C_2 x(t) + D_{21} w(t) + D_{22} u(t) \quad (28)$$

where

$$A = \begin{bmatrix} A_m & 0 & 0 & 0 & 0 & B_m C_{wr} & 0 & 0 & 0 \\ B_{w1}C_m & A_{w1} & 0 & 0 & 0 & B_{w1}D_m C_{wr} - B_{w1}D_p C_{wd} & 0 & & -B_{w1}C_p \\ 0 & 0 & A_{w2} & 0 & 0 & 0 & 0 & 0 & 0 \\ 0 & 0 & 0 & A_{w3} & 0 & 0 & B_{w3}D_p C_{wd} & 0 & B_{w3}C_p \\ 0 & 0 & 0 & 0 & A_{w4} & B_{w4}C_{wr} & -B_{w4}DC_{wd} & -B_{w4}C_{wn} & -B_{w4}C_p \\ 0 & 0 & 0 & 0 & 0 & A_{wr} & 0 & 0 & 0 \\ 0 & 0 & 0 & 0 & 0 & 0 & A_{wd} & 0 & 0 \\ 0 & 0 & 0 & 0 & 0 & 0 & 0 & A_{wn} & 0 \\ 0 & 0 & 0 & 0 & 0 & 0 & B_p C_{wd} & 0 & A_p \end{bmatrix},$$

$$B_1 = \begin{bmatrix} B_m D_{wr} & 0 & 0 \\ B_{w1}D_m D_{wr} & -B_{w1}D_p D_{wd} & 0 \\ 0 & 0 & 0 \\ 0 & B_{w3}D_p D_{wd} & 0 \\ B_{w4}D_{wr} & -B_{w4}D_p D_{wd} & -B_{w4}D_{wn} \\ B_{wr} & 0 & 0 \\ 0 & B_{wd} & 0 \\ 0 & 0 & B_{mn} \\ 0 & B_p D_{wd} & 0 \end{bmatrix}, \quad B_2 = \begin{bmatrix} 0 \\ -B_{w1}D_p \\ B_{w2} \\ B_{w3}D_p \\ -B_{w4}D_p \\ 0 \\ 0 \\ 0 \\ B_p \end{bmatrix}$$

$$C_1 = \begin{bmatrix} D_{w1}C_m & C_{w1} & 0 & 0 & 0 & D_{w1}D_m C_{wr} - D_{w1}D_p C_{wd} & 0 & -D_{w1}C_p \\ 0 & 0 & C_{w2} & 0 & 0 & 0 & 0 & 0 & 0 \\ 0 & 0 & 0 & C_{w3} & 0 & 0 & D_{w3}D_p C_{wd} & 0 & D_{w3}C_p \\ 0 & 0 & 0 & 0 & C_{w4} & D_{w4}C_{wr} & -D_{w4}D_p C_{wd} & -D_{w4}C_{wn} & -D_{w4}C_p \end{bmatrix},$$

$$C_2 = [0 \quad 0 \quad 0 \quad 0 \quad 0 \quad C_{wr} \quad -D_p C_{wd} \quad -C_{wn} \quad -C_p],$$

$$D_{11} = \begin{bmatrix} D_{w1}D_m D_{wr} & -D_{w1}D_p D_{wd} & 0 \\ 0 & 0 & 0 \\ 0 & D_{w3}D_p D_{wd} & 0 \\ D_{w4}D_{wr} & -D_{w4}D_p D_{wd} & -D_{w4}D_{wn} \end{bmatrix}, \quad D_{12} = \begin{bmatrix} -D_{w4}D_p \\ D_{w2} \\ D_{w3}D_p \\ -D_{w4}D_p \end{bmatrix},$$

$$D_{21} = [D_{wr} \quad -D_p D_{wd} \quad -D_{wn}], \quad D_{22} = [-D_p] \quad (29)$$

3.2 Two-degree-of-freedom H_∞ control problem

We suggest a modified two-degree-of-freedom control structure as shown in Fig. 4. The feedforward controller K_1 is primarily to improve tracking performance and the feedback controller K_2 is to reject the disturbance and to robustly stabilize the plant G.

Compared with the conventional structure, the controller K_1 in the feedforward loop is located inside the closed-loop in the modified structure. In the modified structure, W_2 is selected as a high-pass filter or constant to suppress the high frequency components to enter the plant, while W_4 is selected as a low-pass filter to improve the steady state accuracy. All weighting functions and the desired closed-loop model in Fig. 4 serve the same purposes as those in Fig. 2. In Fig. 4, the

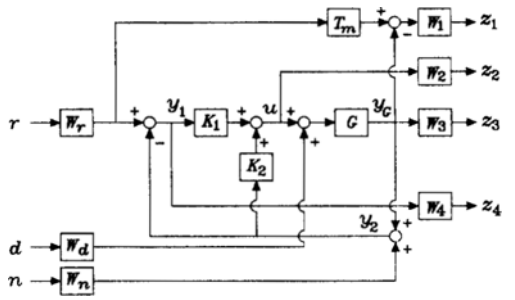

Fig. 4 Two-degree-of-freedom H_∞ control problem.

controlled output y_G and the control input u are given by

$$y_G = GS_i'K_1W_r r + GS_i'W_d d + GS_i'(-K_1+K_2)W_n n \quad (30)$$

$$u = S_i'K_1W_r r + S_i'(-K_1+K_2)GW_d d + S_i'(-K_1+K_2)W_n n \quad (31)$$

where $S_i' = \{I-(-K_1+K_2)G\}^{-1}$.

The exogenous output vectors are given by

$$z_1 = W_1(T_m W_r r - y_G) = W_1(T_m - GS_i'K_1)W_r r - W_1GS_i'W_d d - W_1GS_i'(-K_1+K_2)W_n n, \quad (32)$$

$$z_2 = W_2 u = W_2S_i'K_1W_r r + W_2S_i'(-K_1+K_2)GW_d d + W_2S_i'(-K_1+K_2)W_n n \quad (33)$$

$$z_3 = W_3 y_G = W_3GS_i'K_1W_r r + W_3GS_i'W_d d + W_3GS_i'(-K_1+K_2)W_n n \quad (34)$$

$$z_4 = W_4(W_r r - y_G - W_n n) = W_4(I-GS_i'K_1)W_r r - W_4GS_i'W_d d - W_4\{I+GS_i'(-K_1+K_2)\}W_n n \quad (35)$$

From Eqs. (32)—(35), we obtain the cost transfer function from $w=[r^T d^T n^T]^T$ to $z=[z_1^T\ z_2^T\ z_3^T\ z_4^T]^T$ as

$$T_{zw} = \begin{bmatrix} W_1(T_m - GS_i'K_1)W_r & -W_1GS_i'W_d & -W_1GS_i'(-K_1+K_2)W_n \\ W_2S_i'K_1W_r & W_2S_i'(-K_1+K_2)GW_d & W_2S_i'(-K_1+K_2)W_n \\ W_3GS_i'K_1W_r & W_3GS_i'W_d & W_3GS_i'(-K_1+K_2)W_n \\ W_4(I-GS_i'K_1)W_r & -W_4GS_i'W_d & -W_4\{I+GS_i'(-K_1+K_2)\}W_n \end{bmatrix} \quad (36)$$

If we represent Eq. (36) into linear fractional transformation shown in Fig. 3, the elements of P are given by

$$P_{11} = \begin{bmatrix} W_1T_mW_r & -W_1GW_d & 0 \\ 0 & 0 & 0 \\ 0 & W_3G & 0 \\ W_4W_r & -W_4GW_d & -W_4W_n \end{bmatrix}, \quad P_{12} = \begin{bmatrix} -W_1G \\ W_2 \\ W_3G \\ -W_4G \end{bmatrix},$$

$$P_{21} = \begin{bmatrix} W_r & -GW_d & -W_n \\ 0 & GW_d & W_n \end{bmatrix}, \quad P_{22} = \begin{bmatrix} -G \\ G \end{bmatrix} \quad (37)$$

Note that Eq. (37) are the same as Eq. (19) except that the second rows of P_{21} and P_{22} are added in Eq. (37). By recalling Eqs. (20)—(25), a state space realization of P such that Eqs. (26)—(28) is obtained as follows:

A, B_1, B_2, C_1, D_{11}, and D_{12} are exactly the same as those of Eq. (29). C_2, D_{21}, and D_{22} contain the second rows compared with those of Eq. (29) as shown in the following matrices.

$$C_2 = \begin{bmatrix} 0&0&0&0&0&C_{wr}&-D_pC_{wd}&-C_{wn}&-C_p \\ 0&0&0&0&0&0&D_pC_{wd}&C_{wn}&C_p \end{bmatrix}$$

$$D_{21} = \begin{bmatrix} D_{wr} & -D_pD_{wd} & -D_{wn} \\ 0 & D_pD_{wd} & D_{wn} \end{bmatrix}, \quad D_{22} = \begin{bmatrix} -D_p \\ D_p \end{bmatrix}$$

4. H_∞ Controller Design

4.1 Design specifications

One of performance requirements is to obtain zero steady state error to step reference inputs in each channel. Since there exists an integrator in each channel of the seeker scan loop, it is not necessary to augment an additional integrator. Another requirement is to reject disturbances at low frequency region, and is expressed as follows:

$$\|e\|_2 \le 0.1 \text{ for } \omega < 0.1 \text{ rad/sec whenever } \|d\|_2 \le 1 \text{ or } \|r\|_2 \le 1. \quad (38)$$

The above requirement indicates that at frequencies less than 0.1 rad/sec, the closed-loop system should reject disturbances at the output by a factor of 10-to-1. Expressed differently, steady-state tracking errors in both channels, due to reference step inputs in either channel should be on the order of 0.1 or smaller. Other performance requirements are to achieve a bandwidth of about 15 rad/s for each channel with little cross coupling between outputs, steady state errors within 10% for the given scan commands, and well damped responses.

4.2 Controller synthesis

The desired closed-loop model should be chosen as low order as possible to fulfil the design

specifications. A diagonal matrix with first-order elements is the first choice for the desired closed-loop model. However, it was found that it had large interaction and mismatch after a long adjustment of weighting functions, based on the observation that the roll-off rate of the system appears to be of order $1/s^2$ in most of the elements of the system and that, for exact model matching, the number of poles and zeros difference should be no less than that of the original system (Gao et al., 1989). Hence the desired closed-loop model is chosen to be the second-order system with $\omega_n=17$ rad/sec and $\zeta=0.8$ to improve the model matching in this H_∞ optimization.

$$T_m=\frac{\omega_n^2}{s^2+2\zeta\omega_n s+\omega_n^2}I_2=\frac{289}{s^2+27.2s+289}I_2, \tag{39}$$

where I_2 denotes 2×2 identity matrix.

The weighting functions in Figs. 2 and 4 are chosen to be square and stable. The performance and stability of the feedback system depend on these weighting functions. The choice of these weighting functions plays a role to ensure the solvability of standard numerical algorithm when solving H_∞ problems. In order to achieve good tracking accuracy, reasonable settling time and overshoot, W_1 is chosen to be a first-order high-gain low-pass filter,

$$W_1=\alpha_1\frac{1.2s+18}{s+0.0012}I_2,\ \alpha_1=1.0. \tag{40}$$

This weighting function puts comparatively heavy emphasis at low frequencies, thus a good tracking is expected. The zero of the weighting function is related with the settling time and overshoot, which is selected as -15 considering design specifications. The actuator penalty weighting W_2 reflects control input magnitude and limits the controller bandwidth by selecting W_2 as a high-pass form. However, a diagonal matrix of constants for W_2 is recommended to avoid a higher-order controller unless the performances degenerate. For the seeker scan loop system, W_2 is chosen considering the maximum permissible magnitude of the control input, $u_{\max}=2.5 volts$.

$$W_2=\alpha_2 I_2,\ \alpha_2=0.12. \tag{41}$$

W_3 is related with the plant unmodeled dynamics such as output multiplicative uncertainty, and adjusts the bandwidth of closed-loop system. A first order high-pass filter is selected to achieve the closed-loop bandwidth of about 15 rad/sec.

$$W_3=\alpha_3\frac{10s+1}{s+1000}I_2,\ \alpha_3=5. \tag{42}$$

To ensure good tracking accuracy and disturbance attenuation at low frequencies, W_4 is chosen as a low-pass filter.

$$W_4=\alpha_4\frac{s+100}{s+0.01}I_2,\ \alpha_4=0.15. \tag{43}$$

W_r can be used for the gain adjustments of each control channel and has a diagonal matrix of constants.

$$W_r=\alpha_4 I_2,\ \alpha_4=1. \tag{44}$$

W_d is related to disturbances to the system, and usually selected as a diagonal matrix of constants,

$$W_d=\alpha_5 I_2,\ \alpha_5=0.002. \tag{45}$$

W_n has a diagonal matrix of constants in order to take into account a very small measurement noise.

$$W_n=\alpha_6 I_2,\ \alpha_6=0.0001. \tag{46}$$

The above weighting functions produce satisfactory performances for both control problems. The optimal values, $\gamma_{\min}$, for one- and two-degree-of-freedom control problems are obtained as 1.63 and 1.50, respectively. Suboptimal controllers for $\gamma=1.7$ and 1.6 are selected for one- and two-degree-of-freedom control problems, respectively.

5. Simulation Results

The performance and robustness are evaluated and compared for two H_∞ controllers. In this section, we will denote H_∞ controllers designed using one- and two-degree-of-freedom control structures by ODOF and TDOF, respectively.

5.1 Frequency responses

Figure 5 indicates that the command following performances of ODOF and TDOF are good at low frequencies and the bandwidth requirement is

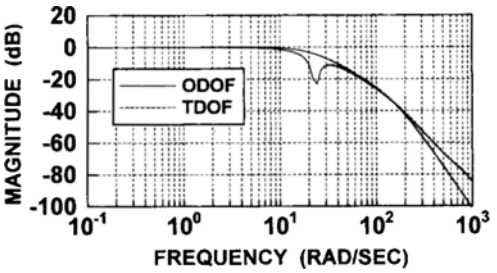

Fig. 5 Command following performance.

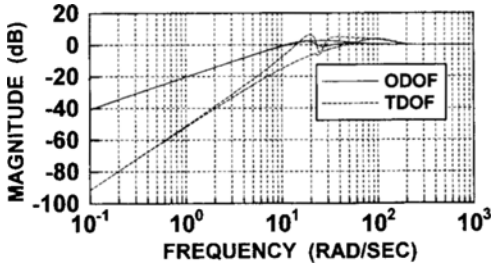

Fig. 6 Disturbance rejection performance.

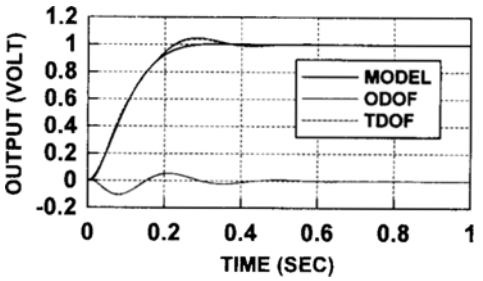

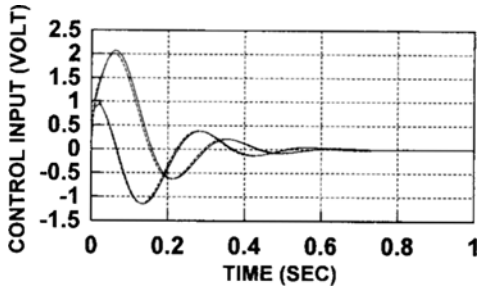

Fig. 7 Time responses to $[1\ 0]^T$ step reference input.

achieved in both controllers.

The sensitivity to the output disturbances is shown in Fig. 6, which shows an acceptable shape for the required performance and the effect of the output disturbance at low frequencies is shown to be small. TDOF offers better disturbance rejection performance than ODOF at low frequencies.

5.2 Time responses

The plant outputs and control inputs to $[1\ 0]^T$ step reference input are shown in Fig. 7, together with the output by the desired closed-loop model, T_m.

Time responses by ODOF and TDOF are very similar. The plant outputs are well coincident with the desired outputs. Maximum coupling ratios between plant outputs are about 9%, where the coupling ratio is defined as the percentage ratio of the peak value of the other channel output to the unit step input applied to one channel. The multivariable interaction between outputs channels is very small and it is due to the desired closed-loop model which is completely uncoupled. Figure 8 shows the plant outputs and control inputs to $[1\ 1]^T$ step reference input. Time responses follow well the desired closed-loop responses and the transient characteristics

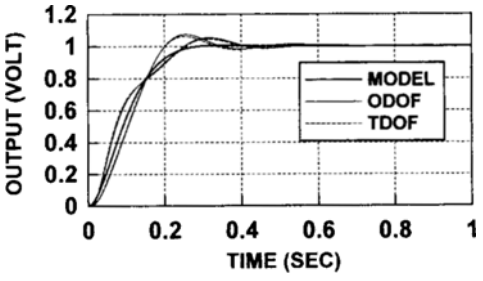

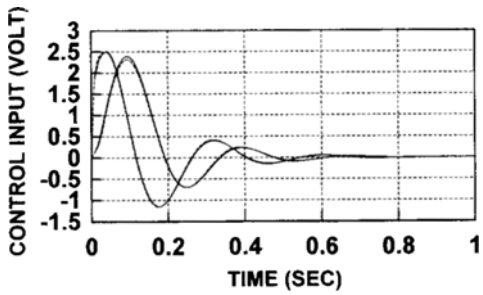

Fig. 8 Time responses to $[1\ 1]^T$ step reference input.

are satisfactory. The control inputs are within the maximum permissible magnitude, $u_{max}=2.5$ volts.

5.3 Scanning performances

Three kinds of scan pattern such as conical, rosette, and spiral scan patterns are designed to enlarge the field-of-view of the seeker during

scanning a target. The command inputs for generating three scan patterns are obtained as follows:

Conical scan pattern

$$R_x(t) = f \cos \theta(t) \quad (47)$$
$$R_y(t) = f \sin \theta(t) \quad (48)$$

Rosette scan pattern

$$R_x(t) = 2f \cos 3(\theta)t - f \cos \theta(t) \quad (49)$$
$$R_y(t) = 2f \sin 3\theta(t) + f \sin \theta(t) \quad (50)$$

Spiral scan pattern

$$R_x(t) = (f/\pi)\theta(t) \cos \theta(t) \quad (51)$$
$$R_y(t) = (f/\pi)\theta(t) \sin \theta(t) \quad (52)$$

where f denotes instantaneous field-of-view.

5.3.1 Model uncertainty

For the seeker scan loop plant, there exists several sources to cause modeling errors. As the look angle of the gyro with respect to the missile centerline increases, the spinning rate of the gyro also increases. Normally, the look angle of the gyro is not zero during both scanning and target tracking phases. This shifts the carrier frequency of the signal processor which was assumed to be synchronized with the constant spinning frequency of the gyro. Therefore the pole and gain of the base-band model of the band pass filter (BPF) are different from the nominal value $a_1 = -50.3$. Thus we assume that uncertainties are involved with the pole of the base-band model of the BPF (Hwang et al., 1995). Note that this pole affects system stability dominantly.

5.3.2 Scanning performance evaluation

The nominal and perturbed responses to three scan patterns are shown in Figs. 9-14, together with reference scanning commands.

The performance robustness is evaluated when the nominal pole of BPF is perturbed by-25. This value corresponds to the percentage deviation of 50% from its nominal value. For scanning performances of ODOF, the nominal responses are good, but the perturbed responses are not satisfactory because at that time the steady state errors are beyond 10% for conical scan command. For scanning performances of TDOF, the nominal and perturbed responses are very similar to each

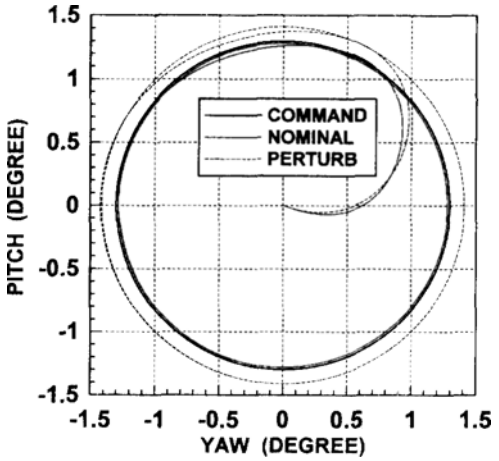

Fig. 9 Conical scanning peformance for ODOF.

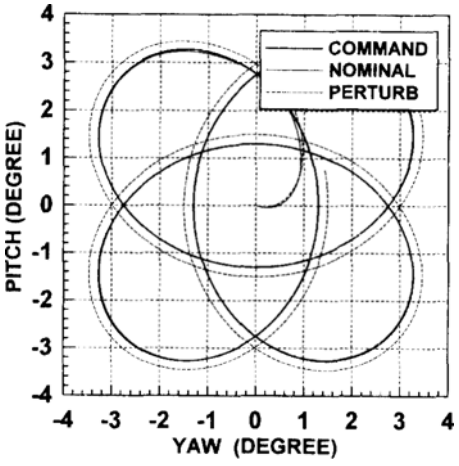

Fig. 10 Rosette scanning peformance for ODOF.

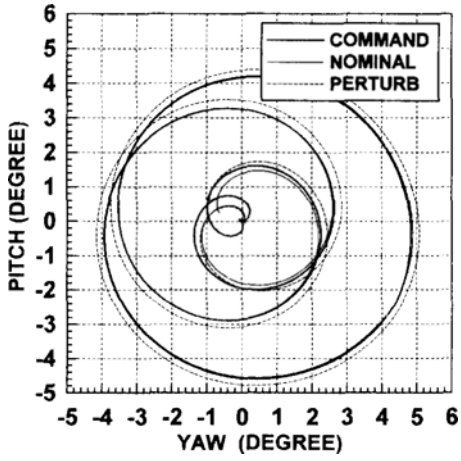

Fig. 11 Spiral scanning peformance for ODOF.

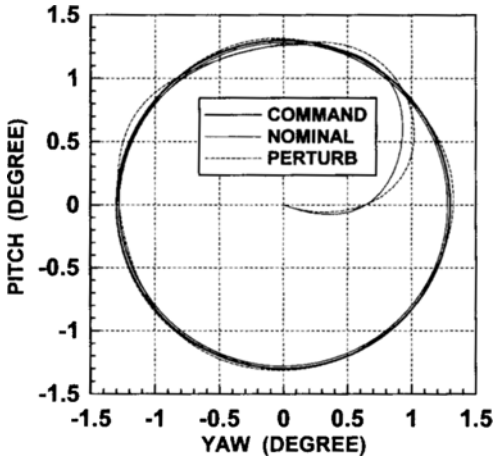

Fig. 12 Conical scanning peformance for TDOF.

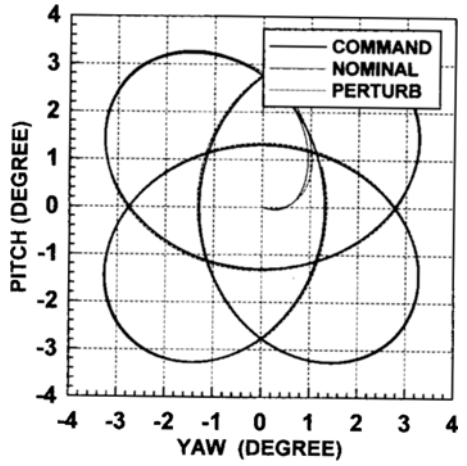

Fig. 13 Rosette scanning peformance for TDOF.

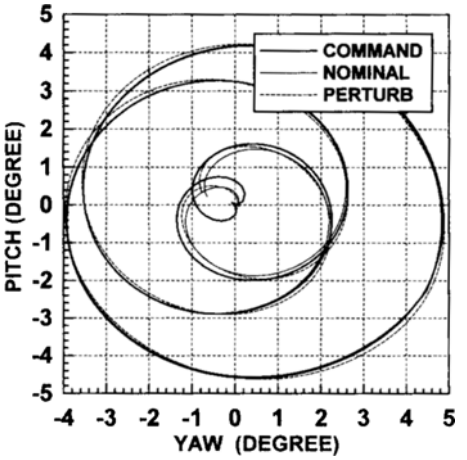

Fig. 14 Spiral scanning peformance for TDOF.

other despite the model uncertainty. Thus the closed-loop system with TDOF is more robust to model uncertainty than that with ODOF, while the former controller structure is more complex.

6. Conclusions

Two H_∞ controllers for a seeker scan loop system have been presented for the purpose of improving scanning performances. The controllers have been designed in the framework of the standard H_∞ optimization problem by combining the mixed sensitivity and model matching problems. The proposed H_∞ control problems can deal with not only frequency domain specifications but also time domain ones such as multivariable interaction between output channels, contrary to the mixed sensitivity problem. In particular, a new two-degree-of-freedom control structure was also introduced to enable better control performance.

The proposed H_∞ controllers satisfy the design requirements, and especially show good scanning performances for three scan patterns. The two-degree-of-freedom H_∞ controller shows better performance and robustness than one-degree-of-freedom H_∞ controller, but both controllers are very effective for the seeker scan loop system.

References

Doyle, J. C., Glover, K., Khargonekar, P. P., and Francis, B. A., 1989, "State-Space Solutions to Standard H_2 and H_∞ Control Problems," *IEEE Transaction on Automatic Control,* Vol. 34, No. 8, pp. 831~847.

Gao, Z., and Antsaklis, P. J., 1989, "On Stable Solutions of the One and Two-Sided Model Matching Problem," *IEEE Transaction on Automatic Control,* Vol. AC-34, pp. 978~982.

Ho, D. W. C., Lam, J., and Chan, T. W. K., 1992, "An Application of H_∞ Design to Model-Following," *International Journal of Control,* Vol. 55, No. 2, pp. 483~509.

Hwang, H. Y. and Lee, H. P., 1993, "Modeling and LQG/LTR Compensator Design of a Seeker Scan Loop," *Transactions of the Korean Soci-*

ety of Mechanical Engineers, Vol. 17, No. 11, pp. 2730~2741. (in Korea)

Hwang, H. Y. and Schmitendorf, W. E., 1995, "Robust H_∞ Stabilizing Controller for a Seeker Scan Loop System," *International Mechanical Engineering Congress and Exposition, San Francisco,* CA, Nov., pp. 307~313.

Mammar, S., and Duc, G., 1992, "Loop Shaping H_∞ Design Applied to the Robust Stabilization of an Helicopter," *First IEEE Conference on Control Applications,* pp. 806~811.

Tsai, M. C., Geddes, E. J. M., and Postlethwaite, I., 1992, "Pole-Zero Cancellations and Closed-Loop Properties of an H_∞ Mixed Sensitivity Design Problem," *Automatica,* Vol. 28, No. 3, pp. 519~530.

Zames, G., 1981, "Feedback and Optimal Sensitivity: Model Reference Transformations, Multiplicative Seminorms, and Approximate Inverses," *IEEE Transaction on Automatic Control,* Vol. AC-26, No. 2, pp. 301~320.